Original Research

Characterizing wheat and barley growth and phenology using multi-spectral remote sensing for site-specific precision agriculture

Yan Zhao[1,*], Ruizhu Jiang[1], Jason Brider[2], Scott Chapman[3], Andries Potgieter[4,*]

[1]Queensland Alliance for Agriculture and Food Innovation, The University of Queensland, Brisbane, QLD 4072, Australia
[2]Department of Primary Industries, Queensland Government, Toowoomba, QLD 4350, Australia
[3]School of Agriculture and Food Sustainability, The University of Queensland, Brisbane, QLD 4072, Australia
[4]Queensland Alliance for Agriculture and Food Innovation, The University of Queensland, Gatton, QLD 4343, Australia

*Corresponding authors. Yan Zhao, Queensland Alliance for Agriculture and Food Innovation, The University of Queensland, Brisbane, QLD 4072, Australia. E-mail: yan.zhao@uq.edu.au; Andries Potgieter, Queensland Alliance for Agriculture and Food Innovation, The University of Queensland, Gatton, QLD 4343, Australia. E-mail: a.potigieter@uq.edu.au

Handling Editor: Xin-Guang Zhu

Abstract. Crop phenology informs in-season management practices such as fertilizer and pest and disease controls to optimize final yield. However, tracking crop growth stages across spatiotemporal domains remains challenging, particularly in rainfed broadacre systems subject to climatic variability. This study uses sequential high-resolution Sentinel-2 imagery to estimate phenological stages of wheat and barley across the Australian grain cropping region which comprises >20 million ha of production. An analysis pipeline was developed to estimate main crop growth stages using targeted vegetation indices (VI) and statistical model fitting approaches. Model accuracy was validated against biophysical simulated phenology and field observations from diverse environments. Both parametric models and non-parametric models were evaluated to fill data gaps and capture growth dynamics. The double logistic model was selected for its balance of performance and efficiency. Strong alignment was observed between VI-derived features and simulated phenology. Peak and right shoulder features showed high accuracy for estimating stages of flag leaf ($R^2 = 0.61$, root mean square error (RMSE) = 8.67 days) and flowering ($R^2 = 0.7$, RMSE = 7.66 days). Scalability was evaluated at 110 and 73 fields across Australia, for 2021 and 2022 seasons, respectively, showing moderate to high correlations with recorded phenology (flag leaf $R^2 = 0.57$–0.58; flowering $R^2 = 0.7$–0.85). The method also predicted tillering ($R^2 = 0.2$–0.7), maturity ($R^2 = 0.73$–0.85), and harvest ($R^2 = 0.55$–0.66) where these observations were available. These results demonstrate the utility of high-resolution satellite data for estimating crop phenology and supporting zonal in-season agronomic management.

Keywords: phenology; curve fitting; spatiotemporal; cereal crops; precision agriculture

1. INTRODUCTION

Global climate change poses unprecedented challenges to agricultural systems, impacting crop growth patterns and necessitating adaptive management strategies (Lobell et al. 2008, Hammer et al. 2020, Jiang et al. 2021). As the Earth's climate undergoes transformative shifts in temperature, precipitation, and extreme weather events, the agricultural sector must adapt to ensure food security and sustainable practices (Wheeler and von Braun 2013, IPCC 2021). This is particularly important in Australia, characterized by rainfed cropping and susceptibility to climate variations (Collins and Chenu 2021, Wang et al. 2023). Central to this adaptation is an understanding of phenology and its role in determining effective crop management practices.

Phenology is important for characterizing crop growth dynamics of winter cereals (such as wheat and barley) for timely crop management practices. For example, the flag leaf stage marks the end of canopy establishment and is influenced by water, nutrient availability, and presence of disease and pests. Similarly, the flowering stage is critical to grain number establishment and stress around this time greatly impacts final yield (Fischer 2011, Richards et al. 2014, Flohr et al. 2017). Timely and spatially resolved information on such growth stages is invaluable for efficient crop management (Zhao et al. 2020, Potgieter et al. 2021). However, the vast expanse of broad-acre grain cropping (>20 M ha with a geographic extent of >1500 km north–south and 500 to 1500 km east–west in the

east and west of Australia), coupled with the diverse climate and environmental conditions across these regions, introduces significant variations in cereal crop growth across Australia (Richards et al. 2014, Flohr et al. 2017). This diversity results in broad phenological windows for different growth stages, presenting substantial challenges in efficiently quantifying these variations within and across large areas.

Regular crop monitoring is assessed through visual observations, with predictions based on growth scales such as Zadoks et al. (1974) and expected weather conditions. These practices have underpinned traditional phenological studies aimed at understanding crop growth patterns to support in-season decisions (McMaster and Wilhelm 1997, GRDC 2016). These methods are labour intensive, prone to observer variability, and are not scalable to accommodate variability across fields (which may be 100 s of ha in area) or across regions, e.g. to inform scheduling of contract harvesting activities. As such, there is growing interest in complementary approaches, particularly crop models and remote sensing, to deliver timely and spatially comprehensive information.

Crop models such as the Agricultural Production Systems sIMulator (APSIM) have been powerful tools for characterizing crop growth under different genotype (G) and management (M) combinations in face of different environments (E). APSIM is a biophysical cropping systems model that integrates climate data, soil properties, and management practices to simulate crop growth and development. This model facilitates a detailed understanding of the complex interactions that influence crop phenology, thereby supporting the refinement of farm management decisions in response to changing climatic conditions (Keating et al. 2003, Holzworth et al. 2014) and as affected by the genetics of the variety being grown (Zheng et al. 2013). However, APSIM is a point-based analysis. Effective operation of such models requires a comprehensive dataset of environmental variables, which can be challenging to procure on a large scale. This limitation restricts the utility of APSIM and similar models to broad-scale agricultural assessments (Keating et al. 2003). Additionally, the application of outputs from crop models, such as APSIM, for particularly crop growth stages, is contingent upon the availability of weather data specific to the location and field. This dependency hinders the scalability of the simulated variables across multiple fields (Holzworth et al. 2014).

Recent advancements in remote sensing, especially satellites-based systems, have opened new possibilities for large-spatial scale temporal crop growth monitoring (Potgieter et al. 2021). The use of remote sensing for growth stage analysis has been extensively explored, revealing its capacity to surpass the accuracy and scope of traditional assessment methods (Zhang et al. 2003, Sakamoto et al. 2010, Pan et al. 2015, Gao and Zhang 2021). For example, remote sensing has been instrumental in identifying key phenological events such as the onset of the growing season, peak vegetation periods, and the end of the growing season through time-series analysis of vegetation indices (VI) for crops including paddy rice, wheat and other woody species (Sakamoto et al. 2005, Zhang et al. 2006). Curve fitting algorithms like double logistic functions (Li et al. 2019), Fourier decomposition (Sakamoto et al. 2005), and temporal smooth filters such as Savitzky–Golay and Whittaker (Chen et al. 2004) are

commonly applied to delineate representative growth curves from various remote sensing data sources. This fitting step converts the original VI time-series with gaps and noises into a smoothed profile, which is then used to estimate the curves' mathematical features (e.g. local minima, maxima, and curvature) to serve as phenological indicators. Zhang et al. (2003) utilized a piecewise logistic function on the Moderate Resolution Imaging Spectroradiometer (MODIS) VI data to estimate key phenological events of global vegetation, including the 'Green-up onset', 'Maturity onset', 'Senescence onset', and 'Dormancy onset'. Similarly, Manfron et al. (2017) determined winter wheat sowing date in Camargue, France, through peak and minimum values analysis using enhanced vegetation index (EVI) from MODIS. Manfron et al. (2017) related the local maxima and the preceding local minima to crop heading and sowing in winter wheat cropping regions.

While the MODIS data, with its high temporal frequency and long-term availability, has been widely used for detecting phenological events, its relatively coarse spatial resolution (up to 250 m) limits application where spatial heterogeneity within and between fields is important. Studies also noted challenges in using MODIS to resolve phenological signals in regions where crop types and phenology are spatially mixed. In contrast, the Sentinel-2 (S2) mission provides high spatial resolution (10–20 meters) with a 5-day revisit frequency, offering a more suitable platform for detecting field-scale phenological dynamics and capturing within field variability. Several studies have explored the capacity of temporal profiles from S2 for characterizing the growth dynamics in the dryland cropping system in Australia, revealing the overall growth variations in the diverse climate and environment conditions (Xie et al. 2024).

Despite these advances, a gap remains in relating remotely sensed data with specific crop growth stages, e.g. flag leaf appearance and flowering, as observed on the ground (Guo et al. 2016, Sakamoto 2018, Younes et al. 2021). This disconnect highlights the need for further research to bridge the gap between remote sensing observations and actual phenological stages (Younes et al. 2021). By aligning the growth curves represented by remotely sensed indices with direct observations of growth stages, researchers can forge a more integrated and accurate framework for monitoring and managing crop production.

The aim of this study is to utilize high-resolution S2 imagery to track key phenological stages of wheat and barley. This is demonstrated by relating remote sensing-derived temporal profiles to both APSIM-simulated and field-observed crop phenology at a 10-m resolution. The proposed method evaluates the utility of this method in tracking specific growth stages including tillering, flag leaf emergence, flowering, and maturity. Additionally, the study quantifies the spatial variability of these stages within and across fields, permitting a detailed assessment of growth patterns at the sub-field level and enabling more informed and timely agronomic decisions.

2. DATA AND MATERIALS

2.1 Validation sites for crop growth observation

The research was conducted in three trial sites located in Western Australia (WA), South Australia (SA), and north-
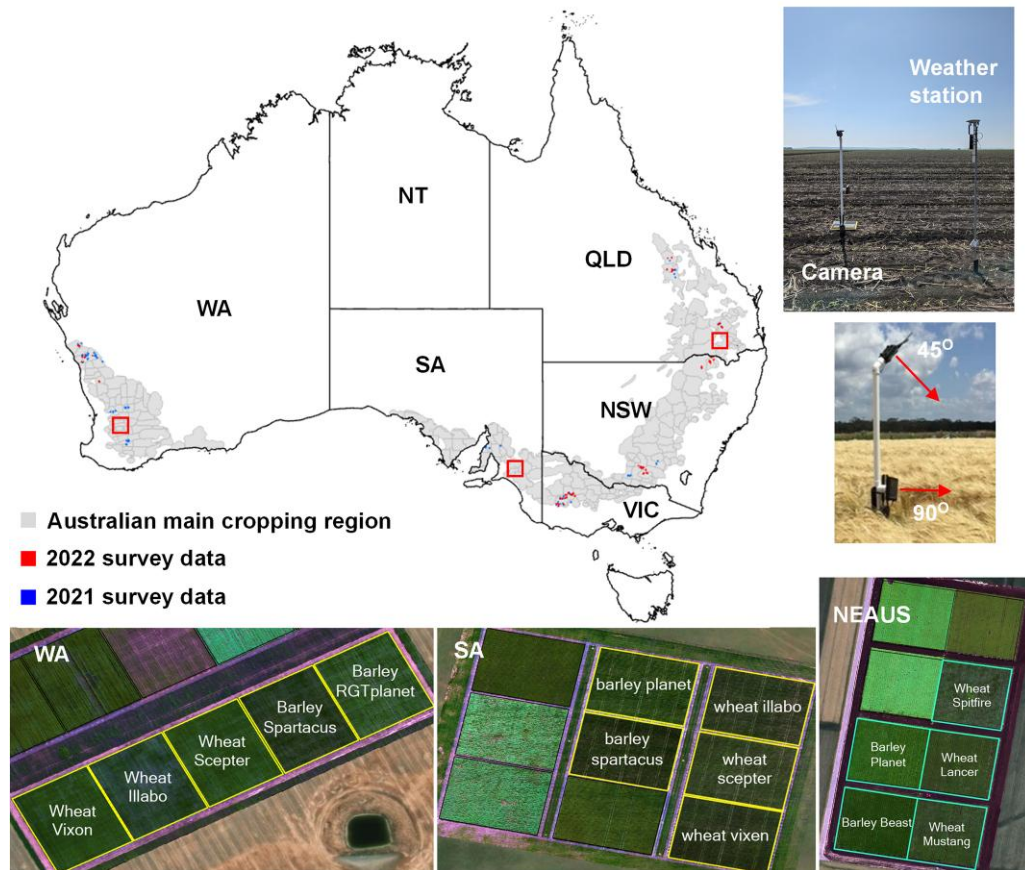
Figure 1. Location of the validation trials and distribution of the national surveyed farms for 2021 and 2022 winter cropping seasons. The validation trials were facilitated with field cameras to record daily canopy development from the canopy top (45° viewing angle) and side (90° viewing angle), and a weather station.

eastern Queensland (QLD), respectively (Fig. 1). These locations encompass a wide range of environmental conditions and agricultural practices, with the trials across two consecutive winter cropping seasons (i.e. 2021 and 2022).

At each site, large square plots measuring 60 by 60 m were established to investigate the growth dynamics of wheat and barley, the two major cereal crops in Australian broadacre farming systems. Wheat cultivars sown included Scepter, Vixen, Illabo, Lancer, and Stealth; and Planet and Spartacus barley varieties were used.

2.2 Field observation for phenology stages

To monitor growth development stages accurately, wildlife cameras (Swift Enduro 4G Trail Camera) were installed to capture the plant/canopy growth from two angles: one at the side of the canopy and another from an above-canopy perspective at a 45° angle. These images were synchronized daily with the PhotoShelter cloud platform (https://www.photoshelter.com/) and then transferred to local computing facilities (Fig. 1). At each site, a micro weather station recorded daily temperatures and rainfall (Arable Mark 2, https://www.arable.com/).

Beyond automated sensor data, regular site visits by a local agronomist provided a record of the main crop growth stages, including emergence, tillering, elongation, flag leaf, flowering, grain filling, and maturity (Fig. 2; Zadoks et al. 1974). For

each plot the Zadoks score is recorded as a decimal code representing the stage at which 50% of plants have reached at the time of the score. The Zadoks score is then converted to text assignment which we use here to describe the stages. The visit frequency varied from weekly to biweekly, influenced by current weather conditions and the stage of growth. To account for potential spatial variability within the 60-m plots, these manual assessments were performed at five distinct locations within each plot.

2.3 Satellite data

To characterize crop growth dynamics for each plot, we developed an automated pipeline to pre-process the S2 imagery through the Google Earth Platform (GEE). S2 provides imagery at 10-m spatial resolution with a 5-day revisit frequency, offering a suitable balance between spatial and temporal resolution for field-scale agricultural monitoring. S2 was preferred to other platforms such as MODIS given the spatial resolution requirements and the specific research objectives of this study. The experimental plots used for validation measures 60 by 60 m. As such, MODIS data (250 m pixels) is not suited to resolve intra-plot variability or align with field-based phenology observations. This study also quantifies within-field phenological variation, a task that benefits from the high spatial fidelity provide by S2. Supplementary Figure S1 demonstrates a comparison of NDVI
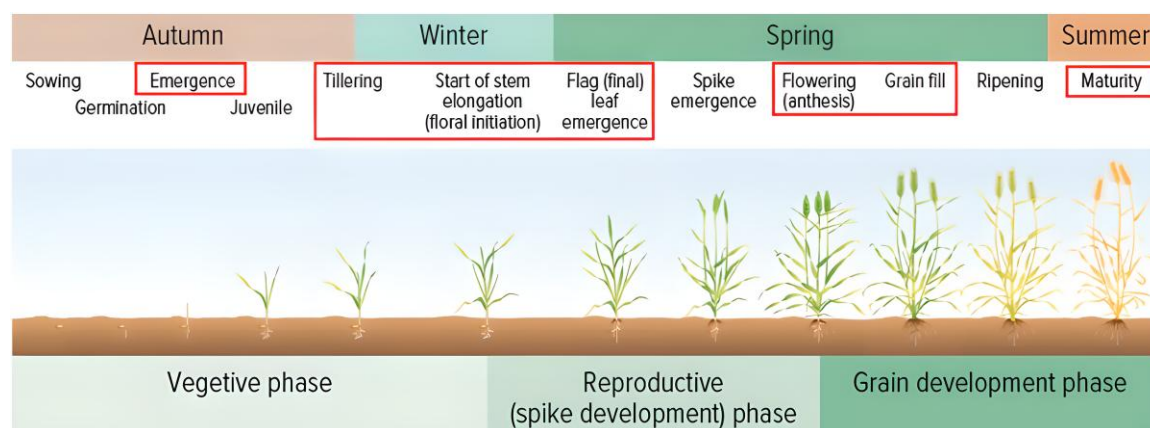
Figure 2. The different growth stages of cereal crops. The rectangle highlighted the target stages studied in this study (Source: GRDC, at https://groundcover.grdc.com.au/crops/cereals/improved-sowing-date-data-to-lift-crop-potential).

profiles derived from MODIS and S2 for representative sites and highlights how the lower-resolution MODIS data smooths out fine scale variability that is clearly captured by S2.

The pre-processing pipeline includes key functions: cloud/shadow masking, calculation of indices, curve fitting, and application of mathematical derivatives for feature extraction for each of the continuous (daily infilled) vegetation crop growth curves. These derivatives are referred to as growth curve features (GCF). Details of specific methodologies for curve fitting and feature extraction techniques are further elaborated in the 'Methods' section.

3. METHODS

Here, we utilized a time series of NDVI to analyse crop growth dynamics. NDVI was selected after comparing the performances of various indices, which characterize the canopy in different aspects (Supplementary Table S1). For example, canopy structure related NDVI, optimized soil-adjusted vegetation index, EVI, and chlorophyll related normalized difference red-edge index, chlorophyll index, and other indices related with moisture (normalized difference water index) and colour (HUE). The index profiles showed subtle differences in capturing the growth dynamics (Supplementary Figures S2 and S3) and has the potential for specific application purposes, for example, flower detection for canola crop using the colour related HUE index (data not shown). To simplify the analysis in this study, the widely accepted NDVI was selected. Features derived from NDVI profiles were correlated with specific growth stages as observed in field data and simulated by APSIM. A key component of the approach is the use of a double logistic algorithm (Li et al. 2019) to address data gaps with the NDVI series (see 3.3). We then calculate features from the curve with mathematical definitions (see 3.4) and examine their relationships with crop growth stages through comparison with APSIM's phenology outputs, and field observations.

3.1 Compiling missing phenology stages from camera photos

The recorded timing of growth stages at several validation sites varied across plots, particularly for certain stages. This

variation, combined with the fact that agronomists were not present daily to monitor each plot, made it difficult to directly align field observations with satellite-derived features. To address this, daily images from field-installed cameras were used to fill in missing stage information and help standardize phenological comparisons. These visual records were used to infer key stages including emergence, early tillering (first tiller with three visible leaves), stem elongation, flag leaf appearance, flowering (or the onset of grain filling), and full maturity (Fig. 2; Supplementary Figure S4).

The process involved using the available field records and camera images as reference points for each main stage. For plots not directly observed at a given stage, images from slightly earlier or later dates were reviewed to identify the date that best matched the target growth stage. This method was carefully adapted to account for phenological differences between wheat and barley, particularly in their flowering stages. Notably, barley's flowering occurs with the head in the sheath, making it less visible compared to wheat, where flowering is marked by the presence of yellow anthers hanging freely from the ear.

3.2 Simulated crop growth stages and thermal time accumulations

The APSIM cropping systems model was used to simulate crop growth and phenological stages for the known wheat and barley varieties (Scepter, Vixen, and Illabo for wheat, and Planet and Spartacus for barley). Each simulation incorporated key management and environmental inputs, including sowing date, plant density, soil type, and fertilizer application. Daily weather inputs were sourced from nearby Bureau of Meteorology (BoM) stations (www.bom.gov.au), including maximum and minimum temperature, rainfall, and solar radiation. These inputs enabled APSIM to generate detailed growth profiles and corresponding phenological stages, providing a robust basis for comparison with both field observations and satellite-derived features.

A central component of the APSIM output is the calculation of thermal time, which denotes the cumulative thermal requirement for each growth stage and its transitions. Thermal time is one of the main driven factors of crop phenological stages

development. It is calculated from the daily average of maximum and minimum crown temperatures, and is adjusted by genetic and environmental factors (Zheng et al. 2015). In this study, the metric serves as a vital reference for correlating S2 VI profiles with specific crop growth stages, thereby enhancing the accuracy of growth stage determination through remote sensing data.

3.3 Generate continuous crop growth through curve fitting

While S2 satellite imagery is pivotal for monitoring vegetation health through a wide range of spectral indices, its 5-day revisit interval and susceptibility to atmospheric interferences, such as cloud cover, often lead to gaps in time series data. To address this, we applied curve fitting methods to reconstruct daily crop growth profiles for each pixel and plot. This study compares several data filling techniques, including Harmonic, Gaussian, Gaussian Process regression (GPR), Spline, and Generalized Additive Model (GAM). Detailed comparisons are provided in Supplementary Figures S1 and S2.

Harmonic fitting, which models seasonal variation using sine and cosine functions, captured general periodic trends but performed poorly near the start/end of season and during canopy saturation, limiting its utility (https://developers.google.com/earth-engine/tutorials/community/time-series-modeling). GPR, a flexible non-parametric method that incorporates prediction uncertainty, was prone to overfitting and computationally demanding on large datasets (Belda et al. 2020, De Caro et al. 2023). Spline methods, which fit piecewise polynomials, were efficient and handled complex data patterns but introduced artefacts and showed sensitivity to missing data (Vorobiova and Chernov 2017). GAM allowed flexible, non-linear modelling through smooth functions, but required careful tuning to avoid overfitting and were also computationally intensive (Wellington et al. 2023). It can effectively capture complex and varying growth patterns, but its flexibility requires careful selection of smoothing parameters to avoid overfitting.

In contrast, the double logistic regression method stood out for its computational efficiency and ability to retain key crop growth dynamics (Vorobiova and Chernov 2017, Li et al. 2019). It models NDVI progression using two logistic functions—one for green-up and one for senescence:

$$f(t) = v1 + v2 \times \left(\frac{1}{1 + e^{-m1(t-n1)}} - \frac{1}{1 + e^{-m2(t-n2)}} \right) \quad (1)$$

where $f(t)$ represents the fitted NDVI value at day t, $v1$, and $v2$ denote the background NDVI and its amplitude over the year, and parameters $m1$, $n1$, $m2$, and $n2$ describe the green-up and senescence phases, respectively.

To parameterize the model, we initially performed harmonic fitting on the Google Earth Engine (GEE) to estimate the season's structure and locate the NDVI peak (Fig. 3A). This enabled segmentation of the NDVI series into two phases—green-up and senescence, allowing separate parameterization for each growth phase (Fig. 3B and C). This method effectively captures complex growth patterns, avoid overfitting, and is well suited to GEE-based large-scale implementations.

3.4 Derive growth curve features from fitted growth profile

This study derived nine distinct GCFs from the fitted daily NDVI profiles to evaluate their alignment with key crop phenological stages observed at the trial sites. Rather than assuming that each feature represents a specific stage, the features were assessed relative to the recorded crop development stages to identify which points on the NDVI trajectory consistently correspond to major transitions in growth. Given the strong relationship between canopy development and NDVI, specific inflection points, slopes and maxima within the curve were evaluated as potential indicators of phenological progression (Fig. 4; Supplementary Figure S4). The GCFs include:

- Start of Season (SoS): the initial rise in NDVI by 1% of the seasonal amplitude; generally aligned with crop emergence in field observations (Supplementary Figure S4).
- Greening onset (G): The inflection point of greatest curvature following SoS. It is typically associated with the onset of tillering and early canopy development.
- D1: the steepest positive slope prior to the peak, most often observed during the stem elongation stage.
- Left Shoulder (L): The point of maximum curvature before the peak, where NDVI increase begins to slow. It closely aligned with full canopy development and primarily linked with flag leaf emergence (Supplementary Figure S4).
- Peak: The maximum NDVI value, indicating full canopy cover. In this study, the peak typically followed flag leaf emergence and preceded flowering, though timing varied by crop and location.
- Right Shoulder (R): The point of greatest curvature following the peak; field data showed this feature closely aligned with flowering to early grain filling, especially in wheat.
- D2: the steepest negative slope during senescence commonly linked with late grain development stages.
- Senescence (S): Marks the phase when the decrease in NDVI slows, aligning with physiological maturity.
- End of Season (EoS): the return of NDVI to near-baseline level broadly corresponding to crop harvest.

3.5 Contrasting of growth curve features with observed data and simulated growth stages

To evaluate the relationship between NDVI-derived GCFs and specific crop growth stages, we first aligned the timing of each feature with the accumulated thermal time from APSIM simulations at each validation site. This allowed us to compare the APSIM-simulated phenology stages with the curve-derived features and subsequently with field-observed phenology. Through this alignment, we tested whether the NDVI-derived features show statistically significant correlations with the actual growth stages recorded in the field (Zhang et al. 2006, Lobell et al. 2015).

The use of a biophysical crop model like APSIM, which closely replicate the phenological development of wheat and barley, is crucial in the analysis of satellite-derived indicators, particularly when direct field observations are limited or unavailable. By ensuring that the simulated growth stages reflect
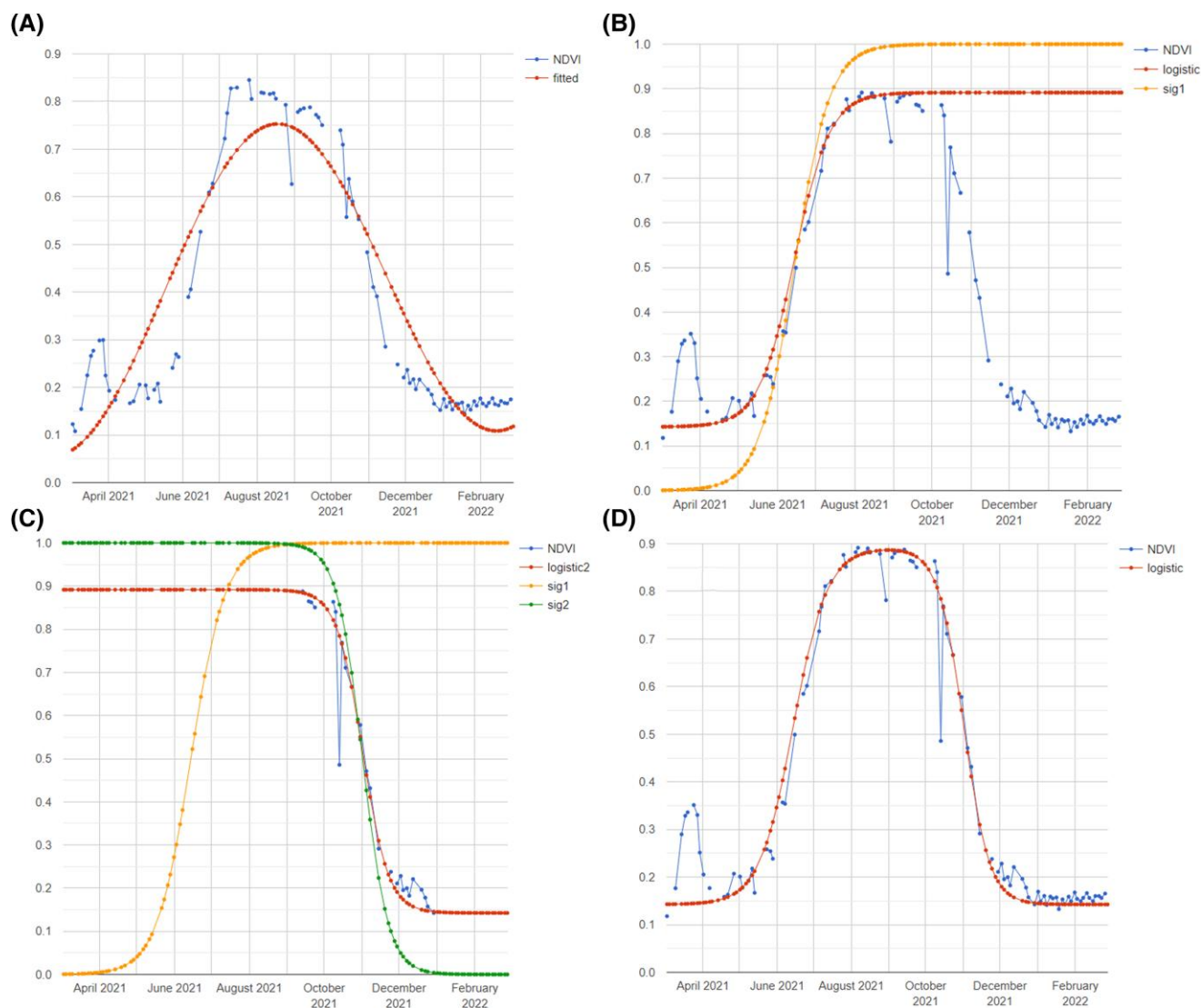
Figure 3. Strategy for fitting the double logistic function to Sentinel-2 NDVI data at trial site in Queensland, 2021 (lat/lon [−28.061, 151.964]): (A) the crop growth cycle is initially split into two segments using harmonic fitting to capture the overall seasonal pattern, (B) a logistic curve is fitted to the green-up phase (first half), (C) a logistic curve is fitted to the senescence phase (second half), and (D) the two segments are merged to form the complete fitted growth curve.
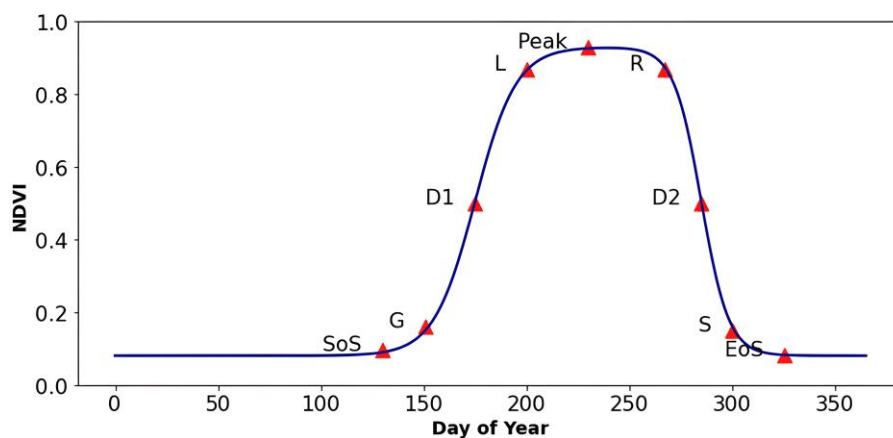

Figure 4. The nine growth curve features (GCF) derived using the double logistic fitted daily NDVI profiles.

actual crop development, we improve the interpretability and reliability of satellite-based estimates. This alignment compensates for the lack of ground-truth data, enabling more robust assessments of crop performance and growth patterns under various climatic scenarios (Heinicke et al. 2022, Poole et al. 2022). The intent of this analysis is to be able to implement solutions using only weather and satellite data, without relying on routine field-based agronomy observations.

3.6 Validation with observed phenology stages at field scale across Australia

To independently validate the relationships between NDVI-derived GCFs and crop phenology, we utilized field-scale phenology observations from commercial agronomy datasets across Australia. The data, provided by Data Farming Pty Ltd, included 110 fields for 2021 season and 73 fields for 2022 season. Due to differences in data structure: descriptive phenology records in 2021 versus Zadoks growth stage scores in 2022, the datasets were analysed separately. For both seasons, the S2 processing pipeline described earlier was used to extract curve features averaged for each field, including key inflection points and slope-derived indicators from fitted NDVI profiles. This comparison provided an independent test of the method's ability to generalize across diverse environments, crop types, and data formats beyond the original trial sites.

3.7 Statistical analysis

For statistical comparison of the curve features against field observations at the validation sites, we employed Analysis of Variance (ANOVA) and paired t-tests. ANOVA was utilized to assess whether variations in curve features were statistically significant across different growth stages. This involved decomposing the total variability into between-group and within-group components to determine whether specific curve features aligned consistently with distinct phenological stages. Subsequently, paired t-tests were applied to examine the differences between the NDVI-derived curve features and the directly observed growth stages at each site. This test compares the means of two related groups to determine if there are statistically significant differences between them, thus allowing for a

precise assessment of the accuracy with which NDVI-derived features can predict actual crop growth stages. While the statistical analysis will identify significant correlations between the satellite derived GCF and observations, expected correlations include the main pairs such as the curve peak versus the observed flag leaf, the R feature versus the flowering (or grain filling which closely following the flowering stage).

When comparing the field recorded growth stages across Australia with the results derived from the proposed method, linear correlation analysis and root mean square errors (RMSE) calculations were employed to quantify the overall performance of the proposed method at a diverse range of fields.

4. RESULTS

4.1 Agricultural production systems simulator simulations at the validation sites

The accuracy of two key phenological stages simulated with APSIM were examined, the 'Flag leaf' and the 'Flowering'. The simulated 'Flag leaf' stage demonstrated an overall good agreement with field observations (Fig. 5A), with a high correlation coefficient (R^2) of 0.83 and a RMSE of 5 days. A slight underestimation in the predicted emergence of the flag leaf stage by the APSIM model relative to the actual observations was observed. Meanwhile, the simulated 'Flowering' showed a strong relationship with the observed flowering at the validation plots (Fig. 5B). Specifically, the model's prediction aligned closely with the observed flowering (at around 50% flowering), with a R^2 of 0.83 and relatively small error (RMSE = 5.78 days).

4.2 Contrasting growth curve features with simulated phenology stages

Here, we compared the thermal time requirements of different growth stage targets with the satellite derived GCFs for wheat and barley across sites and seasons. The paired t-tests provided a statistical rigour to evaluate the significance of these correlations (Table 1) and thus ability of using remotely sensing-derived crop growth stages to estimate phenology. When
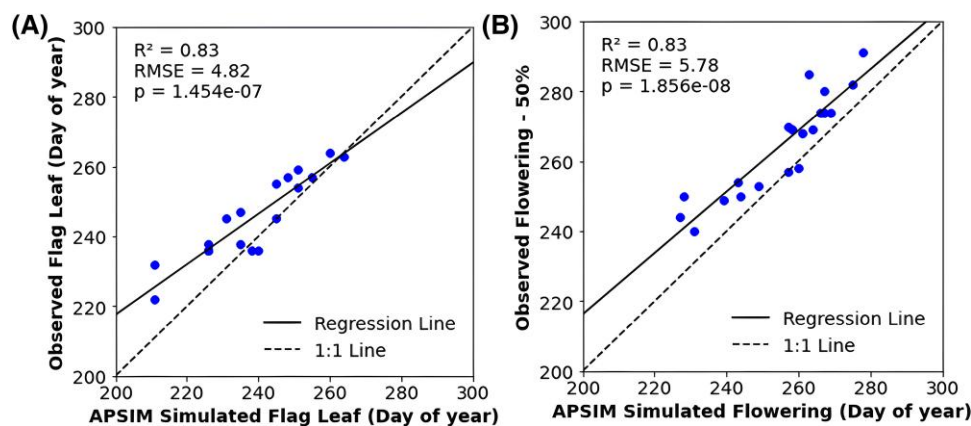

Figure 5. Evaluation of simulated (x-axis) Flag leaf (A) and flowering (B) with field observations. Overall good agreement of simulated flag leaf and flowering with recorded growth stages at the validations sites is observed.

combining wheat and barley data, no significant differences were found for the 'Flagleaf' ($P = 0.535$) and 'Flowering' stages ($P = 0.133$), which implies a close match between the NDVI derived Peak and the simulated stage representing 'FlagLeaf' for these specific stages. This suggests that the accumulation of thermal time for the cereal crops to reach the flag leaf and flowering stages is well-represented by the APSIM model, in line with NDVI observations at (around) peak.

When considering wheat and barley data separately, for wheat, the derived GCF for overall Peak and R remained strong, still showing good indications of the 'Flagleaf' and 'Flowering' stages, respectively. This suggests that the remote sensing-derived features can be potential predictors of these stages for wheat. For barley, the peak feature had good agreement with the simulated 'Flagleaf'. However, the curve-derived

R feature did not show a significant relation with barley 'Flowering'. Instead, the 'StartGrainFill' showed a significant relationship with R, highlighting the distinct differences in the flowering stages of wheat and barley.

Figure 6 shows the comparison of required thermal units to reach different growth stages in wheat and barley, as simulated by APSIM (on the x-axis) and as estimated by a proposed curve-based method (on the y-axis). Overall, the significant correlations, in terms of required thermal units towards each stage, between the two methods affirmed that the identified curve features are closely related to the phenology stage been compared with. For instance, flag leaf is aligned strongly ($R^2 = 0.8$, RMSE = 112) with the GCF representing the peak from the S2 NDVI profile. The curve derived R feature was strongly related to flowering stage, especially for wheat crops ($R^2 = 0.86$, RMSE = 121).

Table 1. The table presents a statistical comparison between APSIM simulated growth stages and curve-derived features for wheat and barley.

Stages APSIM vs curve-derived	T-statistic	P-value	Crop category
Emergence vs SoS	2.20	0.055	Wheat + Barley
Flagleaf vs Peak	0.63	0.535	Wheat + Barley
Heading vs Peak	6.16	0.001	Wheat + Barley
Flowering vs R	−2.73	0.133	Wheat + Barley
StartGrainFill vs R	−0.08	0.937	Wheat + Barley
Maturity vs EoS	−1.78	0.126	Wheat + Barley
Emergence vs SoS	1.203	0.315	Wheat
Flagleaf vs Peak	1.706	0.122	Wheat
Heading vs Peak	6.164	0.001	Wheat
Flowering vs Peak	−0.722	0.489	Wheat
StartGrainFill vs R	2.734	0.023	Wheat
Maturity vs EoS	−1.834	0.126	Wheat
Emergence vs SoS	1.901	0.116	Barley
Flagleaf vs Peak	−1.375	0.202	Barley
Flowering vs R	−3.148	0.012	Barley
StartGrainFill vs R	−2.064	0.069	Barley

The comparisons were assessed using *t*-statistics and *P*-values to determine the significance of the differences between the paired variables. Significant differences were identified at three levels of *P*-values: 0.01, 0.05, and 0.10.

4.3 Relationships of curve derived features with observed phenology stages

Overall, appreciably high agreement was evident between the derived GCF with observed phenology stages at the validation sites (Fig. 7). For example, the curve-derived 'L' feature had a strong positive relationship with the observed stem elongation ($R^2 = 0.61$, RMSE = 8.67 days), which is a critical stage for yield formation before the full crop canopy (Kronenberg et al. 2017). Observed flag leaf stage showed significantly strong correlation with the peak from the S2 NDVI curve ($R^2 = 0.70$, RMSE = 7.66), further affirming the robustness of the mathematically NDVI-derived peak in representing full canopy for estimating the flag leaf stage. Additionally, Fig. 7C indicated a slightly lower but still substantial correlation of 0.69 between observed flowering and the curve derived feature 'R', with an RMSE of around 10 days.

The variations in correlation and RMSE across the plots may reflect environmental heterogeneity and differing crop responses at the sites. However, the overall agreement observed in these plots supports the use of remote sensing data as an effective proxy for field observations, which can be particularly
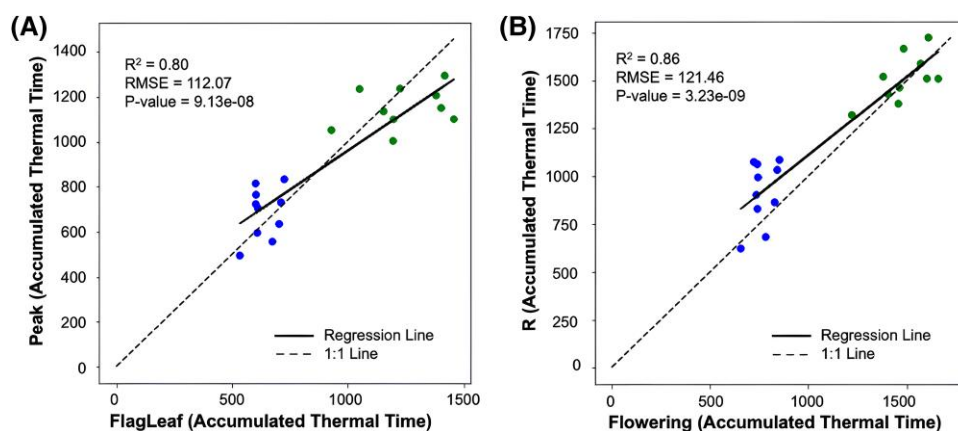

Figure 6. Comparison of the required thermal units for wheat (green) and barley (blue) to the different growth stages revealed with APSIM (x-axis) and proposed curve-based method (y-axis). Higher thermal time requirement for wheat is observed. The overall agreement from the two different sources of results suggests the timing of the curve peak (A) and the right-side shoulder (B) is corresponding to the Flag leaf and flowering stages, respectively.
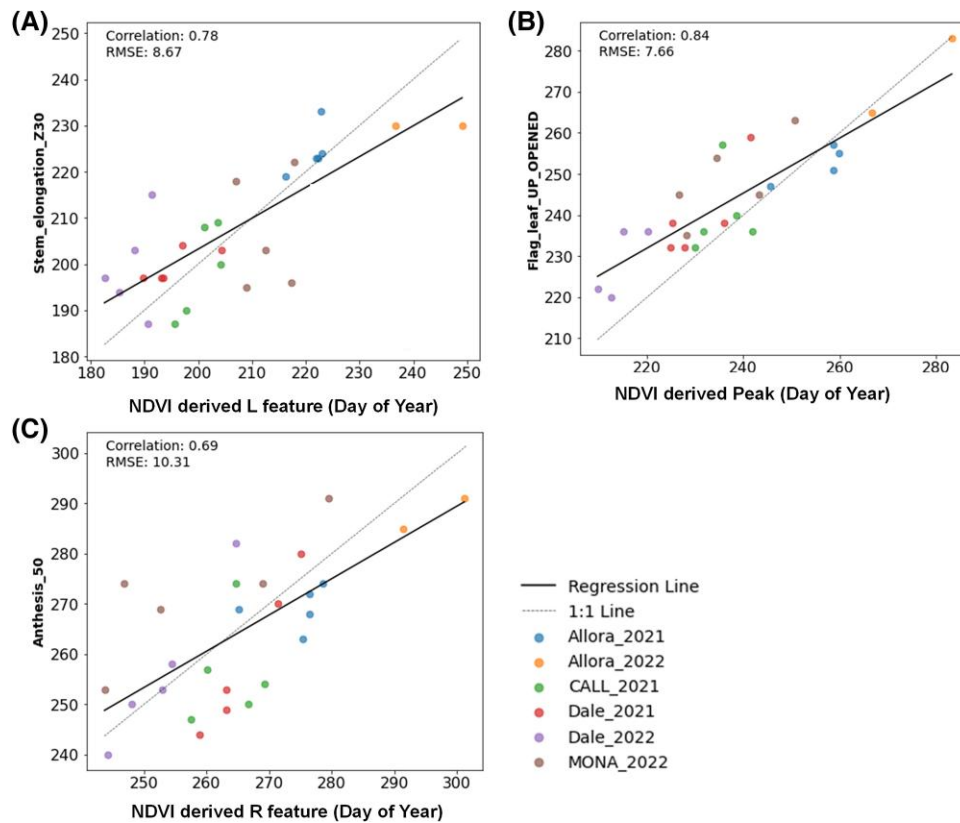
Figure 7. Comparison of curve derived features with observed growth stage at the validation sites. The scatter plots are denoting the relationships of the curve derived left shoulder feature 'L' (A), peak (B), and right shoulder feature 'R' (C) versus the observed stem elongation, flag leaf, and flowering, respectively.

advantageous for large-scale agricultural monitoring where direct field measurements are not feasible.

4.4 Validation analysis with independent fields across Australia

The validation analysis for the 2021 and 2022 winter crop growing seasons incorporated independent field data, providing a robust framework for evaluating the predictive strength of the remote sensing-derived curve features. The scatter plots for both years illustrate the relationship between curve features, such as the NDVI peak, and recorded phenological stages across several fields (Figs. 8 and 9).

In the 2021 season, the correlation coefficients and the linearity of the data points suggest that certain features have a significantly strong association with specific phenological stages (Fig. 8). For instance, the feature representing the NDVI peak aligns well with the flag leaf stage, with a moderate R^2 value (0.58) indicating a reasonable level of predictability. Other features, like the derived R feature, showed a significantly high correlation to flowering ($R^2 = 0.85$, RMSE = 13.07), thus supporting at their potential as reliable markers for these phases of crop development. The features (S and EoS) at the end of the NDVI profile are relating strongly to crop maturity (S, $R^2 = 0.85$) and harvest (EoS, $R^2 = 0.55$), when compared to the respective records in the field.

Application of the developed approach to the 2022 season field surveyed data echoed similar significantly strong relationships between remote sensing derived GCF and observed phenology at a filed scale (Fig. 9). Despite some variability, the general trend across the field scale data demonstrated an appreciably strong agreement between the remote sensing data and field observations, confirming the application of these curve features for objective and rapid monitoring of crop growth for wheat and barley at field scales across seasons and regions.

5. DISCUSSION

5.1 Growth curve derived features can indicate phenological stages

A key finding here is the effective application of GCF extracted from S2 imagery to identify specific phenological stages of the main winter cereal crops (i.e. wheat and barley) in Australia. The double logistic fitting method effectively addressed data gaps and smoothed the NDVI time series, allowing for the identification of subtle changes in crop canopy and detailed characterization of crop growth dynamics. The fitted curve captures the essential growth phases of the crops, including the rapid increase in NDVI during the initial growth stage, the plateau at full canopy development, and the subsequent decline during senescence (Zhang et al. 2003, Li et al. 2019). After comparing with other popular fitting algorithms (Supplementary Figures S1 and S2), including Gaussian, Gaussian Process Regression, Spline, and Generalized Adaptive Model, the double logistic
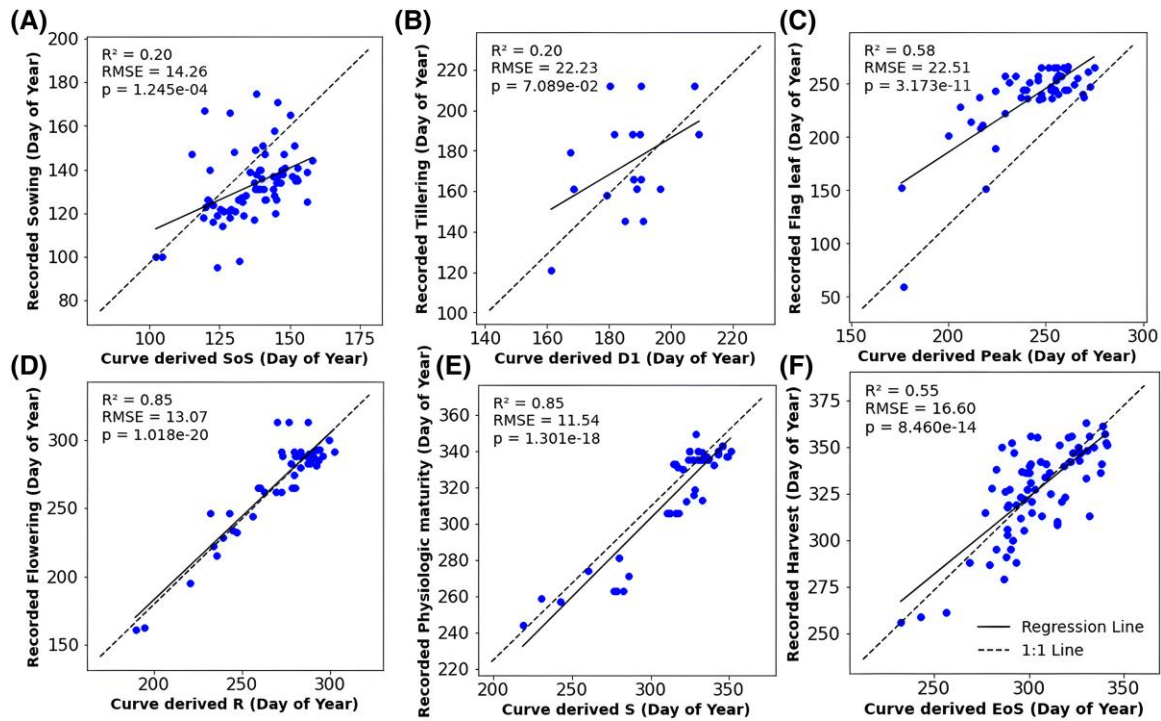
Figure 8. Relationships of curve derived features with observed growth stages recorded at the provided wheat and barley fields across Australia cropping region for the 2021 winter cropping season. The curve derived peak and R features showing strong correlations with the observed flag leaf and flowering stages (C and D), which supports well the findings at the validation sites. Significant high correlations between curve-derived S feature and maturity (E), EoS feature, and harvest (F) are also observed.
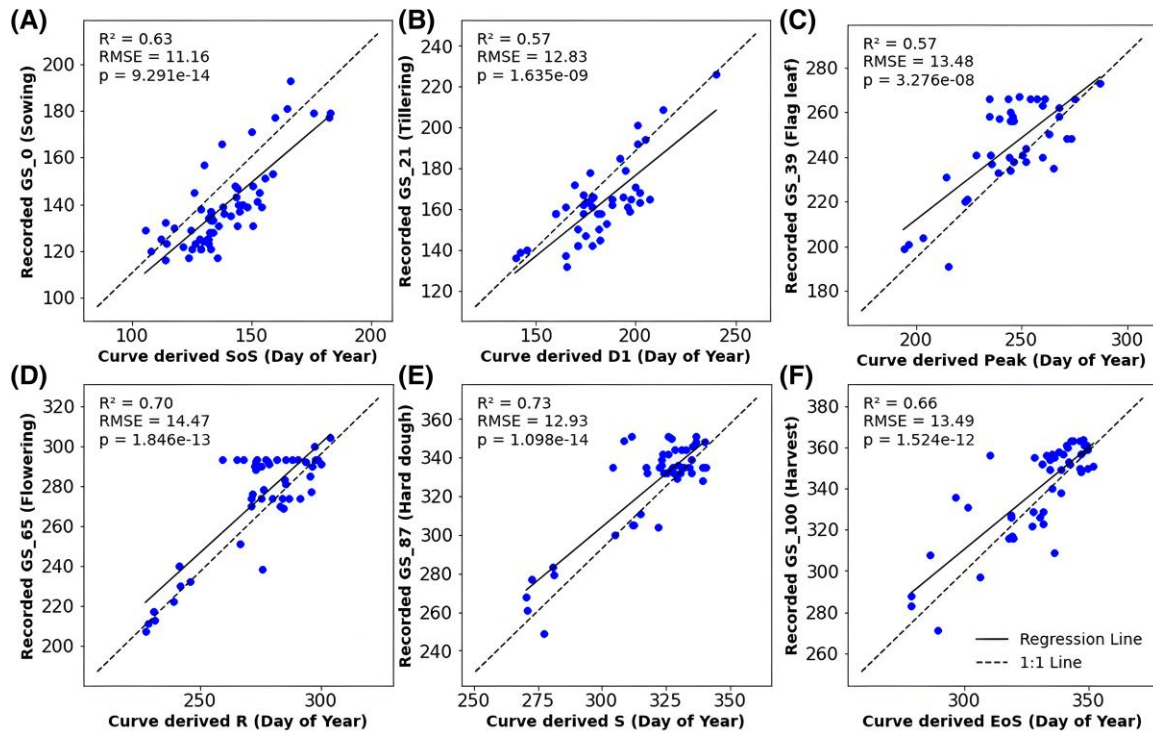

Figure 9. Relationships of curve derived features with observed growth stages recorded at the provided wheat and barley fields across Australia cropping region for the 2022 winter cropping season. The 2022 dataset is recorded with Zadoks growth scores (GS), which provides more specific information about the stage. While the strong correlation of curve derived peak and R with flag leaf and flowering persists (C, D), relationships of curve derived feature D1 (B), S (E), and EoS (F) with recorded tillering (GS21), hard dough (GS 87), and harvest (GS100) are observed.

method showed promising performance in addressing the gaps. More importantly, it is computationally efficient, making it suitable for large-scale analysis using cloud platforms like GEE. This efficiency is crucial for processing large volumes of satellite data and generating timely insights for agricultural management (Chen et al. 2004, Li et al. 2019).

Based on the fitted growth profiles, this research corroborated the efficacy of the proposed approach to accurately estimate the main development stages of cereal growth from high-resolution remote sensing. These phenological stages include critical growth targets like the flag leaf, flowering, and the onset of grain filling. The NDVI peak showed strong correlation with the flag leaf stage, which typically coincides with near maximum green leaf area index. The right shoulder of the NDVI curve was strongly associated with the flowering stage and the commencement of grain filling (when grain number is finalized), both are essential for determining crop yield. These relationships upheld across different environmental conditions and both wheat and barley crops across fields distributed national wide (Figs. 8 and 9). The robust correlations observed between remote sensing data and field observations confirm that remotely sensed index profile, such as NDVI, is a reliable indicator of actual crop conditions (Perry et al. 2022, Farias et al. 2023) highlighting the potential of satellite imagery in enhancing the temporal and spatial resolution of crop monitoring systems (Atzberger 2013).

This study exemplifies the application of functional mathematical functions fused with high-resolution satellite data from S2to estimate crop growth stages within sub-paddock scales that showed high accuracies when applied to independent fields across Australia at a large scale with spatial variation information. Traditional methods of assessing crop phenology, such as manual observations and the application of accumulated local knowledge, are labour-intensive, subject to human error, and often lack scalability. In contrast, the use of S2-derived NDVI features offers a non-invasive, cost-effective, and scalable solution for monitoring crop phenology across vast agricultural landscapes. The high temporal resolution of S2, with its 5-day revisit period, ensures frequent monitoring of crop development, capturing dynamic changes in growth stages that traditional methods might miss.

5.2 Aligning simulations of phenology, thermal time with remote sensing derived features

The APSIM simulations performed well at the validation sites, showing a high correlation with field observed stages and small errors for the varieties tested here. The model's outputted thermal time provided critical information for interpreting the growth curve represented with S2 temporal profile and the derived curve features. The study found significant correlations between the accumulated thermal units (with corresponding estimated growth stage) and NDVI-derived features, such as the alignment of the NDVI peak with the flag leaf and the right shoulder of the curve with the flowering stage. This data science assay provided further validation of the proposed GCF approach for accurately and rapidly estimating and extrapolating phenology observation at point-scale to field, farm and regional scales. By aligning simulated growth stages, thermal time and the NDVI-derived GCF, the proposed analysis enhances the

precision of growth stage determination, thus facilitating more precise and scalable agricultural monitoring with remotely sensed imagery series (Asseng et al. 2013).

5.3 Implications of applications to better inform crop management decisions

The proposed method allows for the accurate estimation of the main crop growth stages (i.e. Flag leaf, Flowering) within crop fields. As demonstrated in Fig. 10A, the field in Western Australia covers an area of 836 ha. It was planted with wheat for 2021 winter season (sown on 31 May 2021), with the recorded flag leaf and flowering stages on 2 Aug 2021 (day of year 216) and 8 Sep 2021 (day of year 253), respectively. However, substantial differences in crop development were evident from the sampled NDVI profiles from different parts of the fields (Fig. 10B). The mapped curve features proposed in this study captured such spatial variations (Fig. 10C and D). Visualizing of spatial variations in predicted phenology offers a comprehensive spatiotemporal perspective on crop development for on-farm crop management decisions. This spatial heterogeneity is often influenced by variations in soil composition, irrigation patterns, and localized climate effects, which are crucial for optimizing resource distribution (Gao and Zhang 2021). Specifically, this capability will facilitate producers to have a more efficient use of inputs such as water, fertilizers, and pesticides, potentially enhancing overall crop health and yield (Sishodia et al. 2020, Gao and Zhang 2021, Pande and Moharir 2023).

5.4 Limitations of remote sensing-based approach for farmers

The proposed approach is not without challenges. Variability in environmental conditions, differences in crop varieties, and the resolution of satellite imagery can impact the accuracy of NDVI-derived features. Continuous refinement of models and validation techniques is essential to address these challenges. Specifically, while the spatial resolution of S2 marks a significant advancement in remote sensing capabilities, offering valuable insights into crop phenology across diverse agricultural landscapes, it also presents specific limitations for farmers:

- Spatial resolution: In regions characterized by fragmented fields and small-scale farming practices, S2's 10 m resolution might not suffice to capture the minutiae of phenological variations. These settings demand an even finer spatial granularity to accurately monitor growth stages within each distinct plot.
- Temporal resolution: The 5-day revisit cycle of S2 may not fully align with the rapid pace of certain phenological transitions, particularly in fast-growing crops or during sudden climatic shifts. This misalignment can lead to missed critical growth stages.
- Data gaps: Data gaps due to cloud cover and varying atmospheric conditions further complicate accurate monitoring. While curve-fitting techniques are employed to mitigate these temporal gaps and smooth out NDVI time series data, the simplification inherent in these algorithms may overlook critical phenological indicators.
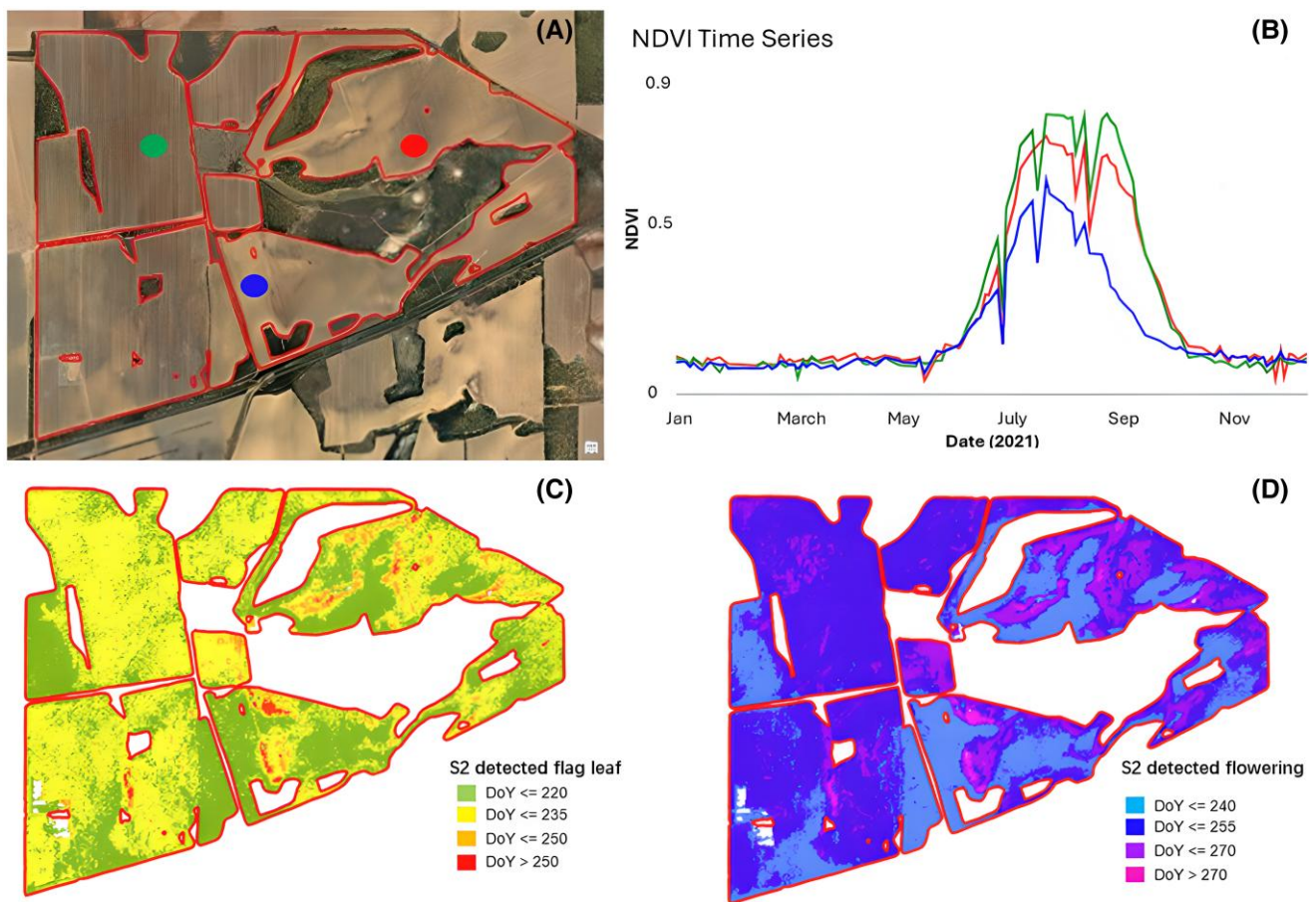
Figure 10. Spatial maps of curve features and the estimated corresponding growth stages derived from Sentinel 2. The blue, red, and green cycles (A) denote the sampled locations inside the field for checking the NDVI profiles (B) with classified maps of (C) flag leaf day of year (DOY) or (D) flowering DOY across the field. Ground-truth observed values were DOY 215 and DOY 253 for flag leaf and flowering, respectively.

- Data volume: The large volume of data generated by high-resolution and frequent remote sensing imagery poses significant challenges in terms of storage, processing, and analysis.

While the first three points above can potentially be addressed by using commercial satellite providers (higher frequency and resolution with fewer data gaps), the utilization of these methods would likely be via specialized service providers who provide data aggregated in ways to match decision support needs. In addition, given that the study combined data from both wheat and barley crops under the broader category of cereal crops, the calibration may not fully account for the nuanced differences in the growth patterns of these distinct crop varieties. As such, crop-specific models could potentially yield more precise estimates given the inherent biological and phenological diversity between wheat and barley across different management and environmental scenarios.

6. CONCLUSION

This study demonstrates the potential of using high-resolution satellite imagery and VI to map crop phenology across vast and diverse agricultural landscapes. The developed approach not only facilitates the identification of in-field growth variations but also offers valuable insights for improving in-season agronomic management, ultimately leading to increased profitability and sustainability in broadacre cropping systems. The scalability and accuracy of the method showcased in this study hold the potential for allowing farmers to make informed decisions, mitigate risks, and optimize resource utilization, thus contributing to a more resilient and productive agricultural sector.

SUPPLEMENTARY DATA

Supplementary data is available at *in silico Plants* online.

Conflict of interest: None declared.

DATA AVAILABILITY

The data underlying this work will be shared on reasonable request to the corresponding authors.

REFERENCES

Asseng S, Ewert F, Rosenzweig C et al. Uncertainty in simulating wheat yields under climate change. *Nat Clim Chang* 2013;**3**:827–32. https://doi.org/10.1038/Nclimate1916

Atzberger C. Advances in remote sensing of agriculture: context description, existing operational monitoring systems and major information needs. *Remote Sens (Basel)* 2013;**5**:4124–4124. https://doi.org/10.3390/rs5084124

Belda S, Pipia L, Morcillo-Pallarés P et al. Optimizing Gaussian process regression for image time series gap-filling and crop monitoring. *Agronomy* 2020;**10**:618. https://doi.org/10.3390/agronomy10050618

Chen J, Jönsson P, Tamura M et al. A simple method for reconstructing a high-quality NDVI time-series data set based on the Savitzky–Golay filter. *Remote Sens Environ* 2004;**91**:332–44. https://doi.org/10.1016/j.rse.2004.03.014

Collins B, Chenu K. Improving productivity of Australian wheat by adapting sowing date and genotype phenology to future climate. *Clim Risk Manag* 2021;**32**:100300. https://doi.org/10.1016/j.crm.2021.100300

De Caro D, Ippolito M, Cannarozzo M et al. Assessing the performance of the Gaussian process regression algorithm to fill gaps in the time-series of daily actual evapotranspiration of different crops in temperate and continental zones using ground and remotely sensed data. *Agric Water Manag* 2023;**290**:108596. https://doi.org/10.1016/j.agwat.2023.108596

Farias GD, Bremm C, Bredemeier C et al. Normalized Difference Vegetation Index (NDVI) for soybean biomass and nutrient uptake estimation in response to production systems and fertilization strategies. *Front Sustain Food Syst* 2023;**6**:959681. https://doi.org/10.3389/fsufs.2022.959681

Fischer RA. Wheat physiology: a review of recent developments. *Crop Pasture Sci* 2011;**62**:95–114. https://doi.org/10.1071/CP10344

Flohr BM, Hunt JR, Kirkegaard JA et al. Water and temperature stress define the optimal flowering period for wheat in south-eastern Australia. *Field Crops Res* 2017;**209**:108–19. https://doi.org/10.1016/j.fcr.2017.04.012

Gao F, Zhang X. Mapping crop phenology in near real-time using satellite remote sensing: challenges and opportunities. *J Remote Sens* 2021;**2021**. https://doi.org/10.34133/2021/8379391

GRDC. *Wheat Northern Region-GrowNotes™*. 2016. https://grdc.com.au/__data/assets/pdf_file/0031/364864/grdc-grownotes-wheatnorthern.pdf (20 August 2025, date last accessed).

Guo L, An N, Wang KC. Reconciling the discrepancy in ground- and satellite-observed trends in the spring phenology of winter wheat in China from 1993 to 2008. *J Geophys Res* 2016;**121**:1027–42. https://doi.org/10.1002/2015jd023969

Hammer GL, McLean G, van Oosterom E et al. Designing crops for adaptation to the drought and high-temperature risks anticipated in future climates. *Crop Sci* 2020;**60**:605–21. https://doi.org/10.1002/csc2.20110

Heinicke S, Frieler K, Jägermeyr J et al. Global gridded crop models underestimate yield responses to droughts and heatwaves. *Environ Res Lett* 2022;**17**:044026. https://doi.org/10.1088/1748-9326/ac592e

Holzworth DP, Huth NI, Devoil PG et al. APSIM—evolution towards a new generation of agricultural systems simulation. *Environ Model Softw* 2014;**62**:327–50. https://doi.org/10.1016/j.envsoft.2014.07.009

IPCC. Technical summary. In: V M-D, Zhai P, Pirani A et al. (eds.) *Climate Change 2021: the Physical Science Basis. Contribution of Working Group I to the Sixth Assessment Report of the Intergovernmental Panel on Climate Change*. Cambridge, UK and New York, NY, USA: Cambridge University Press, 2021, 33–144.

Jiang R, He W, He L et al. Modelling adaptation strategies to reduce adverse impacts of climate change on maize cropping system in Northeast China. *Sci Rep* 2021;**11**:810. https://doi.org/10.1038/s41598-020-79988-3

Keating BA, Carberry PS, Hammer GL et al. An overview of APSIM, a model designed for farming systems simulation. *Eur J Agron* 2003;**18**:267–88. doi: Pii S1161-0301(02)00108-9 Doi 10.1016/S1161-0301(02)00108-9

Kronenberg L, Yu K, Walter A et al. Monitoring the dynamics of wheat stem elongation: genotypes differ at critical stages. *Euphytica* 2017;**213**:157. https://doi.org/10.1007/s10681-017-1940-2

Li X, Zhou Y, Meng L et al. A dataset of 30m annual vegetation phenology indicators (1985–2015) in urban areas of the conterminous United States. *Earth Syst Sci Data* 2019;**11**:881–94. https://doi.org/10.5194/essd-11-881-2019

Lobell DB, Burke MB, Tebaldi C et al. Prioritizing climate change adaptation needs for food security in 2030. *Science* 2008;**319**:607–10. https://doi.org/10.1126/science.1152339

Lobell DB, Thau D, Seifert C et al. A scalable satellite-based crop yield mapper. *Remote Sens Environ* 2015;**164**:324–33. https://doi.org/10.1016/j.rse.2015.04.021

Manfron G, Delmotte S, Busetto L et al. Estimating inter-annual variability in winter wheat sowing dates from satellite time series in Camargue, France. *Int J Appl Earth Obs Geoinf* 2017;**57**:190–201. https://doi.org/10.1016/j.jag.2017.01.001

McMaster GS, Wilhelm WW. Growing degree-days: one equation, two interpretations. *Agric For Meteorol* 1997;**87**:291–300. doi: Doi 10.1016/S0168-1923(97)00027-0

Pan Z, Huang J, Zhou Q et al. Mapping crop phenology using NDVI time-series derived from HJ-1 A/B data. *Int J Appl Earth Obs Geoinf* 2015;**34**:188–97. https://doi.org/10.1016/j.jag.2014.08.011

Pande CB, Moharir KN. Application of hyperspectral remote sensing role in precision farming and sustainable agriculture under climate change: a review. In: Pande CB, Moharir KN, Singh SK et al. (eds), *Climate Change Impacts on Natural Resources, Ecosystems and Agricultural Systems*. 2023, 503–20. https://doi.org/10.1007/978-3-031-19059-9_21

Perry E, Sheffield K, Crawford D et al. Spatial and temporal biomass and growth for grain crops using NDVI time series. *Remote Sens (Basel)* 2022;**14**:3071. https://doi.org/10.3390/rs14133071

Poole N, Sharma R, Nemat OA et al. Sowing the wheat seeds of Afghanistan's future. *Plants People Planet* 2022;**4**:423–31. https://doi.org/10.1002/ppp3.10277

Potgieter AB, Zhao Y, Zarco-Tejada PJ et al. Evolution and application of digital technologies to predict crop type and crop phenology in agriculture. *In Silico Plants* 2021;**3**:diab017. https://doi.org/10.1093/insilicoplants/diab017

Richards RA, Hunt JR, Kirkegaard JA et al. Yield improvement and adaptation of wheat to water-limited environments in Australia-a case study. *Crop Pasture Sci* 2014;**65**:676–89. https://doi.org/10.1071/Cp13426

Sakamoto T. Refined shape model fitting methods for detecting various types of phenological information on major US crops. *ISPRS J Photogramm Remote Sens* 2018;**138**:176–92. https://doi.org/10.1016/j.isprsjprs.2018.02.011

Sakamoto T, Wardlow BD, Gitelson AA et al. A two-step filtering approach for detecting maize and soybean phenology with time-series MODIS data. *Remote Sens Environ* 2010;**114**:2146–59. https://doi.org/10.1016/j.rse.2010.04.019

Sakamoto T, Yokozawa M, Toritani H *et al.* A crop phenology detection method using time-series MODIS data. *Remote Sens Environ* 2005;**96**:366–74. https://doi.org/10.1016/j.rse.2005.03.008

Sishodia RP, Ray RL, Singh SK. Applications of remote sensing in precision agriculture: a review. *Remote Sens (Basel)* 2020;**12**:3136. https://doi.org/10.3390/rs12193136

Vorobiova N, Chernov A. Curve fitting of MODIS NDVI time series in the task of early crops identification by satellite images. *Procedia Eng* 2017;**201**:184–95. https://doi.org/10.1016/j.proeng.2017.09.596

Wang E, Teixeira E, Zheng B *et al.* Modelling climate change impacts on agricultural systems. In: Nendel C (ed.) *Burleigh Dodds Series in Agricultural Science.* Cambridge, UK: Burleigh Dodds Science Publishing, 2023, 481–540. www.bdspublishing.com.

Wellington MJ, Lawes R, Kuhnert P. A framework for modelling spatio-temporal trends in crop production using generalised additive models. *Comput Electron Agric* 2023;**212**:108111. https://doi.org/10.1016/j.compag.2023.108111

Wheeler T, von Braun J. Climate change impacts on global food security. *Science* 2013;**341**:508–13. https://doi.org/10.1126/science.1239402

Xie Z, Zhao Y, Jiang R *et al.* Seasonal dynamics of fallow and cropping lands in the broadacre cropping region of Australia. *Remote Sens Environ* 2024;**305**:114070. https://doi.org/10.1016/j.rse.2024.114070

Younes N, Joyce KE, Maier SW. All models of satellite-derived phenology are wrong, but some are useful: a case study from northern Australia. *Int J Appl Earth Obs Geoinf* 2021;**97**:102285. https://doi.org/10.1016/j.jag.2020.102285

Zadoks JC, Chang TT, Konzak CF. A decimal code for the growth stages of cereals. *Weed Res* 1974;**14**:415–21. https://doi.org/10.1111/j.1365-3180.1974.tb01084.x

Zhang X, Friedl MA, Schaaf CB *et al.* Monitoring vegetation phenology using MODIS. *Remote Sens Environ* 2003;**84**:471–5. https://doi.org/10.1016/S0034-4257(02)00135-9

Zhang X, Friedl MA, Schaaf CB. Global vegetation phenology from Moderate Resolution Imaging Spectroradiometer (MODIS): evaluation of global patterns and comparison with in situ measurements. *J Geophys Res Biogeosci* 2006;**111**:G04017. https://doi.org/10.1029/2006JG000217

Zhao Y, Potgieter AB, Zhang M *et al.* Predicting wheat yield at the field scale by combining high-resolution sentinel-2 satellite imagery and crop modelling. *Remote Sens (Basel)* 2020;**12**:1024. https://doi.org/10.3390/rs12061024

Zheng B, Biddulph B, Li D *et al.* Quantification of the effects of VRN1 and Ppd-D1 to predict spring wheat (Triticum aestivum) heading time across diverse environments. *J Exp Bot* 2013;**64**:3747–61. https://doi.org/10.1093/jxb/ert209

Zheng B, Chenu K, Doherty A *et al. The APSIM–Wheat Module (7.3 R3008).* 2015. https://www.apsim.info/wp-content/uploads/2019/09/WheatDocumentation.pdf (20 August 2025, date last accessed).